Repeated Airborne Laser Scanning for Analyzing Drought-Related Crown Dynamics in Mature Norway spruce

Alice Penanhoat [1], Langning Huo [1]

[1]Department of Forest Resource Management, Swedish University of Agricultural Sciences, S-901 83 Umeå, Sweden – {alice.penanhoat, langning.huo}@slu.se

Keywords: LiDAR, height-increment, crown traits, growth

Abstract

Repeated airborne laser scanning (ALS) offers new opportunities to quantify individual-tree structural dynamics over time. In this study, we analysed annual to multi-year changes in height growth and crown structure of mature Norway spruce in southern Sweden using repeated ALS acquired in 2016, 2017, 2019, and 2022. Individual trees were delineated from normalized point clouds, and tree height increment, maximum crown radial extension, crown projection area, and crown-boundary metrics were derived to evaluate temporal structural change. To interpret the results in relation to recent climate extremes, the observation period was divided into pre-drought (2016–2017), during-drought (2017–2019), and post-drought (2019–2022) phases, and structural changes were expressed on a yearly basis. Tree height increased significantly in all periods. Annualized median height growth was 24.9 cm yr^{-1} before drought, 26.5 cm yr^{-1} during drought, and 16.8 cm yr^{-1} after drought. In contrast, annualized maximum crown radial expansion was limited before drought (2.4 cm yr^{-1}), peaked during drought (19.0 cm yr^{-1}), and was nearly absent after drought (0.17 cm yr^{-1}). Crown-boundary metrics suggested an upward shift of the upper crown and a reorganization of the middle crown over time, lower-crown estimates were more uncertain. Driver analyses showed that height growth was mainly related to tree size before and during drought, whereas post-drought growth became more influenced by stand competition. Overall, this study shows that repeated ALS is a useful tool for analysing crown structural dynamics during and after drought, providing a promising basis for monitoring how tree architecture responds to stress.

1. Introduction

The phenotyping of trees *i.e.* the quantitative measurements of their morphological properties in relation to their performance (Bian et al., 2022) is central to the selection of the phenotypes most suited to the growing conditions, as currently done in forestry breeding programs. Climate change challenges the current phenotyping program, first because the rapids changes in environmental conditions calls for the acceleration of the characterization of the phenotypes, and second by changing the selection criteria. Indeed, tree performance was traditionally assessed by measuring height and diameter (Liziniewicz et al., 2025), reflecting tree competitiveness and productivity. However, competition not only affects absolute growth, but also allocation patterns with lateral growth favoured at the expense of height growth in the case of overtopped trees (Messier and Nikinmaa, 2016; Penanhoat, 2024). Further, the existing trade-off in carbon allocation to growth and non-structural carbon - which includes carbon involved in defence and survival mechanisms; ((Huang et al., 2019) as well as drought tolerance (Souden et al., 2020)- challenges the definition of performance as pest outbreaks and drought frequency increases (Romeiro et al., 2025).

Tree architecture results from the differential growth and allocation strategy in response to the changing environment of the tree, thus reflecting life history (Laurans et al., 2024). For this reason, crown characteristics are used to evaluate breeding properties, wood quality and stress resistance in forestry, as well as to understand ecosystem processes (Pont et al., 2020). In the meantime, architectural traits such as crown projection area are key determinant of a tree productivity (Broeckx et al., 2012) but also vulnerability to stresses.

Traditional ground-based measurements of tree traits are labour-intensive, prone to error, and often reductors in the number of traits described. Thus, studies of crown traits dynamic are scarce, and tree architecture is often described at one point in time. LiDAR, on the other hand, enables an exhaustive description of the 3D structure of trees, and airborne laser scanners enable covering large areas and gaining access to a high number of trees.

Here, we investigate the relation between tree height increment, crown structural traits and competition indices using four years of airborne laser scanning (ALS) conducted before, during and after a drought period.

2. Materials and methods

2.1 Study area

The research was carried out in the Remningstorp area, Sweden (58°27′18″N, 13°39′8″E). The Remingstorp study area is a forest estate located in southern Sweden, encompassing about 1,100 hectares of mainly coniferous hemi-boreal forest, mostly composed of Norway spruce (*Picea abies)*. It serves as an important field site used extensively in forestry research, particularly for provenance trials and forest management studies. The terrain consists of glacial till soils with intermingled hills and plains.

We used 48 circular plots of 15m radius located in mature forest stands dominated by Norway spruce (stands for which spruce represented more than 80% of the standing volume). Stands were located at least 600 meters apart from each other, in stands with trees presenting no signs of declining vitality and located at least 20 meters away from zones identified as damaged by bark-beetles. 24 circular plots of 15 meter radius were established in 2021 during a first campaign (C1), and 24 other plots were established in 2023 (C2, Figure 1). At plot establishment, all trees within the plot were inventoried and their coordinates and diameter at breast height (DBH) were recorded (Huo et al., 2024).

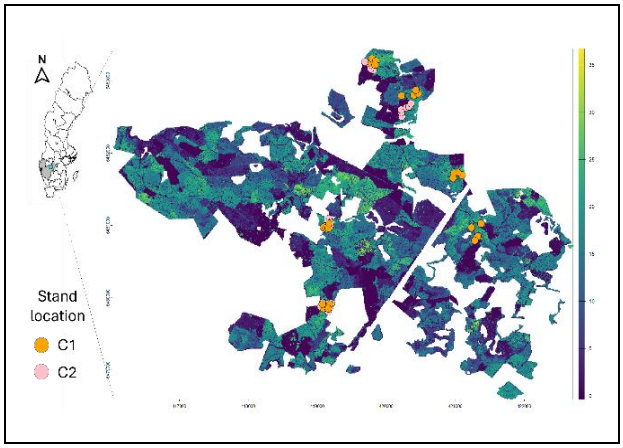

Figure 1. Location of the study site: the Remningstorp forest estate in Southern Sweden and Canopy Height Model (Using the 2022 ALS data) with location of the studied sites for the first (C1, orange) and second campaigns (C2, pink).

2.2 Airborne Laser Scanning

We used airborne laser scanning data (ALS) collected in 2016, 2017, 2019 and 2022 (Table 1). In 2016, ALS data were collected using the Teledyne Optech Titan X multispectral LiDAR system. The scanner operated simultaneously across three wavelengths (532 nm green, 1064 nm near-infrared, and 1550 nm shortwave infrared), and in 2017 ALS data were acquired using the SPL100 single-photon LiDAR system. The scanner operated at a flight altitude of 3800 m above mean sea level, achieving a point density of 25 points per square meter. In 2019, the ALS data were collected in October using the Leica TerrainMapper 2 scanner, which operates at a pulse repetition frequency of up to 2 MHz, with a maximum scan angle ranging between 20° and 40° and a footprint size of ranging between 10 and 15 cm on the ground, and in July 2022 using the Leica CityMapper-2 (Table 1). All ALS data were georeferenced to the Swedish coordinate system SWEREF 99 TM.

Year	Sensor / System	Key Specifications
2016	Teledyne Optech Titan X (multispectral LiDAR)	Three simultaneous wavelengths: 532 nm (green), 1064 nm (NIR), 1550 nm (SWIR)
2017	SPL100 (single-photon LiDAR)	Flight altitude: 3800 m a.s.l.; point density: 25 pts/m²
2019	Leica TerrainMapper 2	Pulse repetition frequency: up to 2 MHz; scan angle: 20°–40°; footprint size: 10–15 cm
2022	Leica CityMapper 2	15 pts/m2

Table 1. ALS information collection

2.3 – Point-cloud processing and tree crowns delineation

For each year, the ALS was segmented into the area of interest using the catalogue function from *lidR* R-package (Roussel et al., 2021), before classifying the points into ground and above-ground returns using the cloth simulation algorithm implemented in the same package. The classified ground-points were used to compute a digital terrain model (DTM) using the triangular irregular network method and a resolution of 0.2 m. The DTM was further used to normalize the heights of each point cloud and compare differences between years.

On the normalized point-clouds, we computed a canopy height model (CHM) with a 0.15 m resolution using the point-to-raster method implemented in the *lidR* package. The resulting CHM was smoothed using a moving window of three-by-three pixels (Figure 2). Finally, we segmented individual trees on the normalized point-cloud using a *lidR* implementation of the individual tree segmentation method developed by (Li et al., 2012). This method detects local maxima and classifies points from highest to lowest as belonging to the same tree or not according to threshold distance parameters.

We used different distance thresholds for the segmentation of the trees (Table 2) for the different years of ALS. These parameters were calibrated by comparison with the field inventory recording the tree positions and diameter at breast height (DBH) for the corresponding point-cloud area.

The inventory resulting from the segmentation of the ALS point cloud was matched to the inventory from the field mapping of tree position using Euclidian distance and attributing to each tree the label corresponding to the closest tree. This was done for each ALS acquisition, enabling the comparison of tree parameters from one year to another.

Year	First Distance threshold (m)	Second distance threshold (m)
2016	2.5	1
2017	2.5	1
2019	0.5	1.1
2022	0.5	1.6

Table 2. Individual tree segmentation parameters

2.3 Crown traits

For each year and for each individual tree point cloud, we calculated the total tree height as the height of the point with the maximal Z. We calculated the crown projection area (cpa) using 2D convex hull fitted on the points projected on the horizontal plane using the *concaveman* R-package (Gombin et al., 2025).

We estimated crown parameters by fitting curves to the crown profile. Such methods enable the description of tree shape (Ferrarese et al., 2015) and the determination of the living crown boundaries (Popescu and Zhao, 2008). Here, we used this method to delineate the upper, middle, and lower crown parts.

First, the tree point cloud was sliced into vertical sections. For 2016 and 2017 point clouds, slices were 25 cm thick, to account for the sparser point cloud density, while for 2019 and 2022, 10-cm-thick slices were used. For each slice, we determined the minimum bounding circle enclosing the set of crown points using the *shotGroups* R-package (Wollschlaeger, 2025). The crown profile corresponded to the distribution of the radii as a function of height, smoothed using a loess function (span = 0.5). On the crown profile, we calculated the first derivative to determine inflection points as points of significant change. Each inflection point determined a crown segment. In a second processing step, we calculated the change in segment radius as the positive

difference between the start and end radius relative to the maximal radius. We iteratively aggregated segments shorter than 80 cm length and with a change in radius below 5% to the preceding segment (from top to bottom).

The final crown parts were defined as top-crown (TC, the uppermost segment with radius increasing downward), lower crown (LC, lowermost segment with radius decreasing downward) and middle crown (MC, segment located between top and lower crown). Further, we defined the total crown as the sum of all crown segments). For each segment, we reported the starting heights (HSC, HMC, HTC; Figure 4). Finally, we included the maximum radius (R_max) and height of maximal radial extension (H_Rmax).

Tree height increment was calculated as the height difference from a LiDAR campaign to the next for each tree point-cloud, and radial increment as the maximal crown radius (R_max) differences between campaigns (Figure 3). For comparison across campaigns, height and crown extension changes were normalized by the length of each observation interval.

2.4 Environmental conditions estimation

Further, for each tree we calculated four competition indices: We calculated the Heygui competition index using (1) heights and (2) crown projected area, which corresponds to the sum of the ratio between the target tree and the neighbours’ size-metric (height or CPA) in a 5-meter radius, weighted by the distance between the target tree and the neighbour. Two other metrics were calculated directly on the stand point-cloud and raster: (3) The crown competition for light (KKL) index, defined as the proportion of the cone volume of the target tree occupied by neighbouring tree crowns (Pretzsch, 1995); and (4) the proportion of canopy area below two-meters in the three-meter buffer around the crown of a target tree. Finally, a moisture index was attributed to each tree as the mean value of intercepting raster cells in a radius of three-meter around the trcee position (Figure 5). We used the 2-meter resolution soil moisture map of Sweden (Larson et al., 2022).

2.5 Statistical processing

All statistical analyses were done in R (version 4.4.3).

We assessed the significance of total tree height change between consecutive time periods using pairwise Wilcoxon signed-rank tests for each year pair (2016–2017, 2017–2019, and 2019–2022), evaluating whether the observed differences were significantly greater than zero.

To test the drivers of tree height increment, we ran linear mixed model using the lme4 package (lme4 package). For the first model, height increment was modelled as a function of a competition index, using each year separately and including PlotID as a random effect. We ran the model using the KKL, the Heygui index calculated on heights, the Heygui index calculated on crown projected area, and the proportion of area not covered by canopy in the 3meter around a tree. For Heygui indices, we included all trees in a five-meter radius. In the second model, soil moisture was included as an additional term, and in the third model, DBH, crown projected area, tree height, and lower boundary of the top crown (HTC) were further included. For each model, the quantile distribution of the residuals was tested using the *DHARMa* R-package (Hartig, 2017).

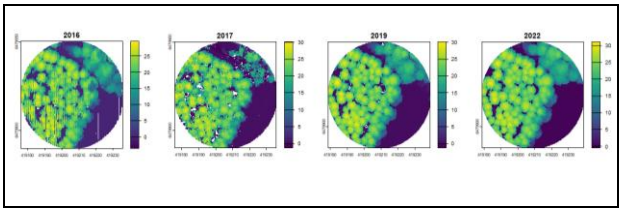

Figure 2. Canopy Height Model in 2016, 2017, 2019 and 2022.

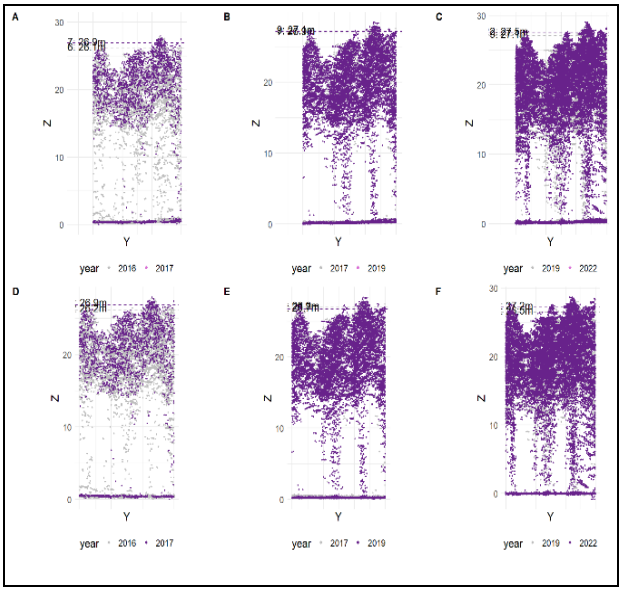

Figure 3. Comparison of the raw point-clouds of the different years; transverse view on a 15 * 15 meter transect for a single plot. The dashed lines indicate the 99 height-percentile in the subset of the point cloud. A-C: Non-normalized point cloud. D-F: Normalized point-cloud.

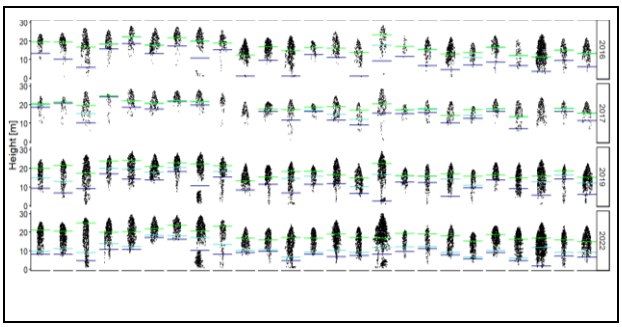

Figure 4. Example of individual tree point clouds segmented in the different years (2016, 2017, 2019, 2022) and the associated classified crown segments indicated by the horizontal lines. Start of the crown (HSC, purple); start of the middle crown (HMC, light blue); start of the upper crown (HTC, green). Illustrative example for 25 different trees.

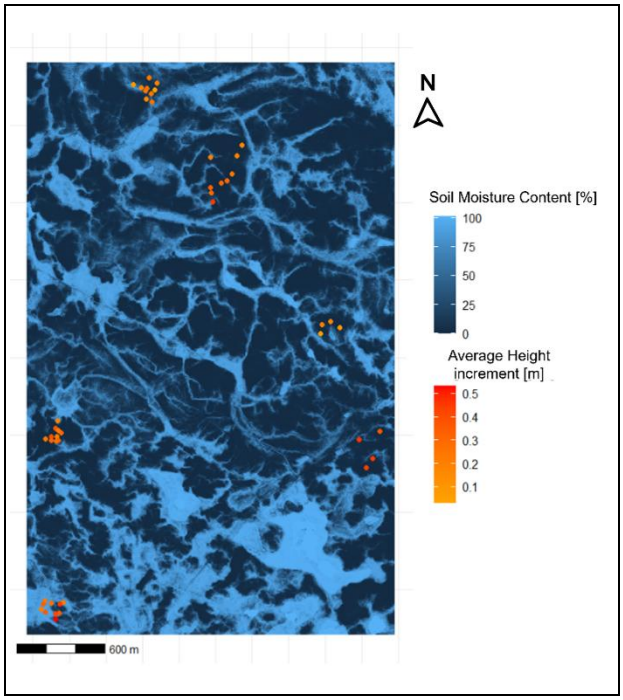

Figure 5. Map of the area and plots (dots) coloured by average individual tree height increment per stand in the pre-drought period (2016-2017).

3. Results

3.1 Height and radial increment

Wilcoxon rank sum tests revealed statistically significant increases in individual tree height between consecutive measurement years. When comparing heights in 2017 and 2016, the test indicated a significant shift towards higher values in 2017 ($p = 0.03$) with a median height increment of 24.9 cm. Likewise, when comparing heights in 2019 and 2017, we observed a highly significant shift ($p < 0.001$) and a median height increment of 53.0 cm, which persisted for the comparison of 2022 heights with 2019 ($p < 0.001$) median height increment 50.4 cm (Figure 6). On the observation period, the average height increment from 2016 to 2022 was of 1.28 m (standard-deviation = 0.86 m).

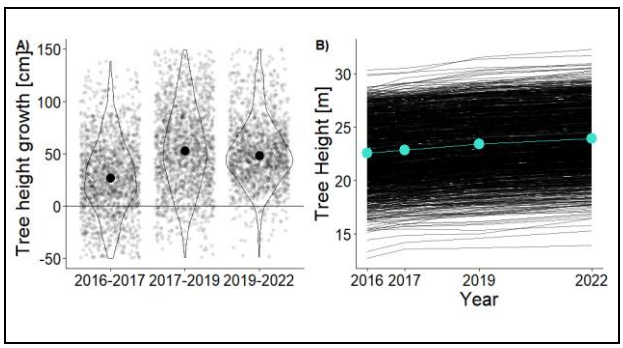

Figure 6. A) Absolute Individual tree height growth measured as height difference measured from ALS; B) Individual tree height trajectory (black lines) and average growth trajectory (blue points).

The comparison of crowns’ maximum radial extension (R_max) between 2016 and 2017 showed no statistically significant difference (Wilcoxon-test, $p = 0.22$). The estimated median difference of 2.4 cm suggests only a slight (non-significant) increase. In contrast, the comparison of R_max values between 2017 and 2019 showed a significant difference ($p < 0.001$) with a median difference of 38.0 cm and a narrow confidence interval (0.344 to 0.415). Finally, the comparison between 2019 and 2022 revealed no significant change ($p = 0.80$), with a negligible median difference of 0.5 cm (Figure 7).

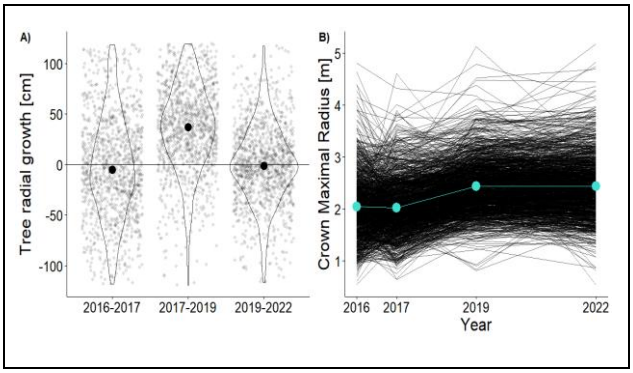

Figure 7. A) Absolute individual tree radial growth as difference in maximal crown extension between two years, B) individual tree trajectory (black lines) and average growth trajectory (blue points).

3.2 Temporal variation in crown boundaries characterization

We compared the crown boundaries estimated at each year. For the lower height of the top crown (Height of start of the top crown; HTC), we found a significant increase (Wilcoxon-test, $p < 0.001$) from 2016 to 2017 and from 2017 to 2019 ($p < 0.001$). For 2019 to 2022, the median paired difference was positive (15.0 cm) but not significant ($p = 0.13$, Fig. 8A). Likewise, we compared the estimation of the lower height of the mid crown (HMC). From 2016 to 2017, we found a significant increase (median paired difference = 1.5 m, $p < 0.001$). However, from 2017 to 2019 the difference was significant ($p < 0.001$) and negative (-1.90 m), as for the difference between 2019 and 2022 (median paired difference = -3.7 m, $p < 0.001$, Figure. 8B).

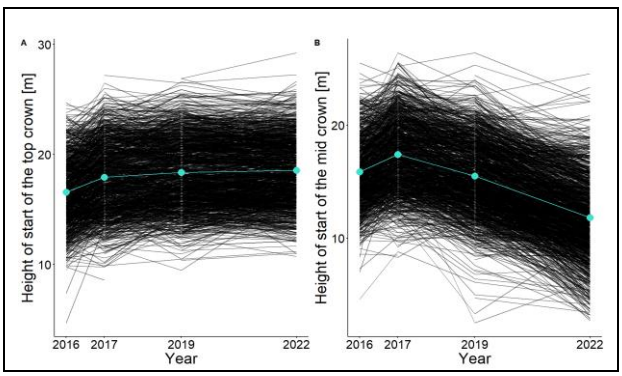

Figure 8. Estimation of the height of A) the start of the top-crown (meters) and B) height of start of the mid crown (meters) for the different years. Black lines indicate single trees trajectories and blue points indicate yearly mean.

3.3 Drivers of tree height increment

In the first model, the effect of the proportion of vegetation cover in the three meter radius around the tree did not have a significant effect on tree height increment on neither of the years (2016 -

2017: estimate = -0.14, p = 0.385, conditional R-squared = 0.06; 2017-2019: estimate = 0.01, p = 0.89, conditional R-squared = 0.11; 2019-2022: estimate = 0.03, p = 0.622, conditional R-squared = 0.05). Likewise, we did not find any significant relation between the KKL index, the Heygui coefficient index calculated on height, the Heygui coefficient index calculated on crown projected area and the tree height increment (Figure 8).
In the second model, including the soil moisture index, we found no significant effect of the explaining variable on the growth, neither from 2016 to 2017 (moisture index: p = 0.28, KKL: p = 0.19) nor from 2017 to 2019 (moisture index: p = 0.11, KKL: p = 0.85). From 2019 to 2022, soil moisture index was not significant (p = 0.87) but KKL had a significant positive effect on height increment from 2019 to 2022 (beta = 1.18 E-3, p < 0.001). Finally, in the third model, the height increment from 2016 to 2017 was significantly and negatively related to crown projected area (beta = -8E-3, p = 0.004), positively and significantly affected by DBH (beta = 0.01, p < 0.001), and negatively affected by tree height (beta = -0.02, p = 0.026). From 2017 to 2019, crown projected area had a significant and negative effect on height increment (beta = -3E-3, p = 0.037), DBH had a significant positive effect (beta = 8E-3, p< 0.001) and tree height a negative significant effect (beta = -9E-3, p = 0.042). Finally, the 2019 to 2022 height increment was significantly and positively affected by KKL (beta = 2E-3, p < 0.001), positively loaded by crown projected area (beta = 2E-3, p = 0.019) and DBH (beta = 2E-3, p = 0.006) and negatively affected by tree height (beta = -9E-3, p < 0.001).

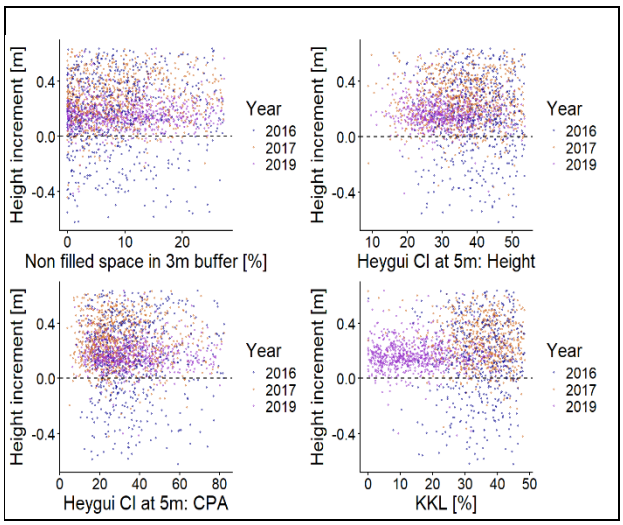

Figure 9. Height increment (meters) as a function of initial crown light competition index (KKL, percentage of downward cone occupied by neighbours).

At stand scale, we found that from 2016 to 2017, basal area (BA) had a positive non-significant effect on mean tree height increment (Coef. Estimate = 0.003, p = 0.18, R-squared = 0.04). From 2016 to 2017, BA had a positive, almost significant effect on average height increment (Coef. Estimate = 0.003, p = 0.06, R-squared = 0.07). However, from 2019 to 2022, the effect of basal area on average tree height growth was negative and almost significant (Coef. Estimate = -0.002, p = 0.06, R-squared = 0.09, Figure 10).

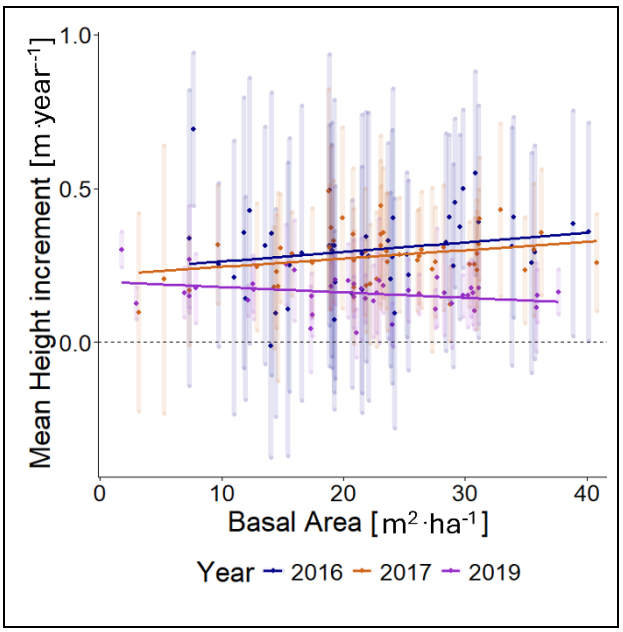

Figure 10. Average stand tree height growth [m] and stand scale and basal area [$m^2.h^{-1}$]. Error bars indicate the 95% confidence interval

3.4 Drought effect on tree height increment and crown expansion

The summer of 2018 was characterized by extreme drought in Northern Europe, including Sweden (Bakke et al., 2020). Thus, we considered the following drought chronology, with 2016–2017 treated as the pre-drought period, 2017–2019 as the during-drought period, and 2019–2022 as the post-drought period. Median annual individual tree height growth equalled 24.9 cm yr^{-1} in the pre-drought period, 26.5 cm yr^{-1} during drought, and 16.8 cm yr^{-1} in the post-drought period. Thus, annual height growth was similar before and during drought, but declined clearly after drought. A similar normalization of maximum crown radial extension (R_max) showed a marked contrast among periods: radial expansion was negligible before drought (2.4 cm yr^{-1}), peaked during drought (19.0 cm yr^{-1}), and was nearly absent after drought (0.17 cm yr^{-1}). This indicates that trees maintained substantial vertical growth before and during drought, whereas the post-drought period was characterized by reduced annual height growth and strongly constrained lateral crown expansion.

The crown-boundary metrics suggest that tree shape changed mainly through an upward shift of the upper crown and a reorganization of the middle crown. At the pre-drought period (2016-2017), both the start of the top crown and the start of the mid crown moved upward, indicating that the crown became more concentrated in the upper part of the tree, i.e. a more elevated and compact crown profile. During the drought (2017-2019), the lower boundary of the top crown continued to rise, while the start of the mid crown shifted downward. This suggests a more differentiated crown shape, with a relatively more elevated upper crown but a deeper middle crown zone. Together with the strong increase in maximum crown radius during 2017–2019, this is consistent with crowns becoming fuller in the middle portion while maintaining upward extension. During the post-drought period (2019-2022), the top-crown boundary no longer changed significantly, whereas the mid-crown boundary

continued to move downward, indicating that the upper crown stabilized while the crown profile became deeper below.
Driver analysis showed that height growth was controlled mainly by tree size before and during drought but became more influenced by stand competition after drought. In 2016–2017 and 2017–2019, competition indices and soil moisture were not significant, whereas DBH had a positive effect and initial tree height and crown projected area had negative effects on height increment. In 2019–2022, KKL became a significant positive predictor of height increment, DBH remained positive, initial height remained negative, and basal area showed a negative near-significant effect at stand scale. Together, these results indicate that post-drought height growth became more constrained by stand context and competition than in the earlier periods.

4. Discussion

We observed a significant change in tree height at the individual scale. In the six years of observation, the average height increment we observed was higher than observed by (Bayer and Pretzsch, 2017) for similar DBH range of spruces but on a reduced number of individuals. Further, we observed significant increases in the height of lower boundary of the tree crown as well as radial extension of the crown. However, for the lower part of the crown, the differences between years reflect differences in the occlusion between years. Indeed, previous studies have highlighted the effect of overstory on LiDAR pulse penetration (Korpela et al., 2012). Thus, the high occlusion of the lower part of the crown as well leads to patterns inconsistent with the biology of spruce trees, for which the self-pruning of dead branches in the lower part of the crown leads to an increase in the height of the start of the living crown (Sharma et al., 2017).

When the competition index was the only explaining variable included, we did not observe a significant effect of initial competition (measured using four different competition indices) on the tree height increment in the following year (Fig. 8). However, the light competition index (KKL) had a significant positive effect on tree growth for the period 2019-2022 when tree traits and soil moisture were further included. This contrasts previous studies showing that increasing competition reduced annual basal area increment (Fraver et al., 2014). Two of the competition indices were calculated using crown polygons resulting from the individual tree segmentation (CI_height, and CI_cpa), thus error in segmentation could result in the calculation of the index. However, the two other indices calculated on the original data showed similar results. The short observation period (less than a year for the minimum observation length from 2016 to 2017) could also explain the small effect observed. At stand scale, the effect of basal area on height increment was also contrasting across years, with a positive effect for both 2016 to 2017 and 2017 to 2019 periods, but a negative effect for the 2019-2022 period.

For all studied periods, we observed a significant negative effect of tree height on height increment, with increasing coefficient from pre- to during to post-drought. In relation to the severe drought and elevated temperatures during the growing season of 2018, this is in line with the difference of resistance to drought stress of smaller trees, more tolerant than taller trees (Camarero et al., 2024). Likewise, on a study on deciduous trees, legacy effects of drought were observed up to six years after the drought event (Orwig and Abrams, 1997).

5. Conclusions

Repeated ALS successfully detected significant structural changes in mature Norway spruce across 2016–2022. After accounting for unequal period lengths, annual height growth was similar before and during drought but declined after drought, while crown radial expansion peaked during drought and was nearly absent afterward. Crown metrics suggest an upward shift of the upper crown and a reorganization of the middle crown, although lower-crown changes remain uncertain because of possible LiDAR occlusion effects. Height growth was mainly related to tree size before and during drought, but became more influenced by competition after drought, with signals consistent with stronger water limitation following the 2021 drought. Overall, repeated ALS can be a useful tool for analysing crown structural dynamics during and after drought, providing new opportunities to monitor how trees adjust their growth and crown architecture across stress and recovery phases.

Acknowledgments

This research was funded by the European Union with project RESDiNET [project grant 101078970 to LH], the Forest Damage Centre at the Swedish University of Agricultural Sciences [project grants 260FDC05, 260FDC57 and 260FDC44 to LH], the Swedish Research Council for Sustainable Development Formas [project grant 2024-00404 to LH].

References

Bakke, S.J., Ionita, M., Tallaksen, L.M., 2020. The 2018 northern European hydrological drought and its drivers in a historical perspective. Hydrology and Earth System Sciences 24, 5621–5653. https://doi.org/10.5194/hess-24-5621-2020

Bayer, D., Pretzsch, H., 2017. Reactions to gap emergence: Norway spruce increases growth while European beech features horizontal space occupation – evidence by repeated 3D TLS measurements. Silva Fennica 51.

Bian, L., Zhang, H., Ge, Y., Čepl, J., Stejskal, J., EL-Kassaby, Y.A., 2022. Closing the gap between phenotyping and genotyping: review of advanced, image-based phenotyping technologies in forestry. Annals of Forest Science 79, 1–21. https://doi.org/10.1186/S13595-022-01143-X/TABLES/1

Broeckx, L.S., Verlinden, M.S., Vangronsveld, J., Ceulemans, R., 2012. Importance of crown architecture for leaf area index of different Populus genotypes in a high-density plantation. Tree Physiol 32, 1214–1226. https://doi.org/10.1093/treephys/tps083

Camarero, J.J., Pizarro, M., Gernandt, D.S., Gazol, A., 2024. Smaller conifers are more resilient to drought. Agricultural and Forest Meteorology 350, 109993. https://doi.org/10.1016/j.agrformet.2024.109993

Ferrarese, J., Affleck, D., Seielstad, C., 2015. Conifer crown profile models from terrestrial laser scanning. Silva Fennica 49.

Fraver, S., D’Amato, A.W., Bradford, J.B., Jonsson, B.G., Jönsson, M., Esseen, P., 2014. Tree growth and competition in an old-growth *Picea abies* forest of boreal Sweden: influence of tree spatial patterning. J Vegetation Science 25, 374–385. https://doi.org/10.1111/jvs.12096

Gombin, J., Vaidyanathan, R., Agafonkin, V., 2025. concaveman: A Very Fast 2D Concave Hull Algorithm.

Hartig, F., 2017. DHARMa: Residual Diagnostics for HierArchical Regession (Multi-Level / Mixed) Regression Models. R package.

Huang, J., Hammerbacher, A., Weinhold, A., Reichelt, M., Gleixner, G., Behrendt, T., van Dam, N.M., Sala, A., Gershenzon, J., Trumbore, S., Hartmann, H., 2019. Eyes on the future – evidence for trade-offs between growth, storage and defense in Norway spruce. New Phytologist 222, 144–158. https://doi.org/10.1111/nph.15522

Huo, L., Persson, H.J., Lindberg, E., 2024. Analyzing the environmental risk factors of European spruce bark beetle damage at the local scale. Eur J Forest Res 143, 985–1000. https://doi.org/10.1007/s10342-024-01662-4

Korpela, I., Hovi, A., Morsdorf, F., 2012. Understory trees in airborne LiDAR data — Selective mapping due to transmission losses and echo-triggering mechanisms. Remote Sensing of Environment 119, 92–104. https://doi.org/10.1016/j.rse.2011.12.011

Larson, J., Lidberg, W., Ågren, A., Laudon, H., 2022. Predicting soil moisture conditions across a heterogeneous boreal catchment using terrain indices. Hydrology and Earth System Sciences 26. https://doi.org/10.5194/hess-26-4837-2022

Laurans, M., Munoz, F., Charles-Dominique, T., Heuret, P., Fortunel, C., Isnard, S., Sabatier, S.-A., Caraglio, Y., Violle, C., 2024. Why incorporate plant architecture into trait-based ecology? Trends in Ecology & Evolution 39, 524–536. https://doi.org/10.1016/j.tree.2023.11.011

Li, W., Guo, Q., Jakubowski, M.K., Kelly, M., 2012. A New Method for Segmenting Individual Trees from the Lidar Point Cloud. Photogrammetric Engineering & Remote Sensing 78, 75–84. https://doi.org/10.14358/PERS.78.1.75

Liziniewicz, M., Almqvist, C., Helmersson, A., Holmström, A., Ene, L.T., 2025. LiDAR-estimated height in a young Scots pine (Pinus sylvestris L.) genetic trial supports high-accuracy early selection for height. Annals of Forest Science 82, 12. https://doi.org/10.1186/s13595-025-01283-w

Messier, C., Nikinmaa, E., 2016. Effects of light availability and sapling size on the growth, biomass allocation, and crown morphology of understory sugar maple, yellow birch, and beech. http://dx.doi.org/10.1080/11956860.2000.11682604 7, 345–356. https://doi.org/10.1080/11956860.2000.11682604

Orwig, D.A., Abrams, M.D., 1997. Variation in radial growth responses to drought among species, site, and canopy strata. Trees 11, 474–484. https://doi.org/10.1007/s004680050110

Penanhoat, A., 2024. Inter and intra-specific interaction effects on individual tree architecture and stand structure, and consequences for ecosystem functions in mixed forests.

Pont, D., Dungey, H.S., Suontama, M., Stovold, G.T., 2020. Spatial Models With Inter-Tree Competition From Airborne Laser Scanning Improve Estimates of Genetic Variance. Front Plant Sci 11, 596315. https://doi.org/10.3389/fpls.2020.596315

Popescu, S.C., Zhao, K., 2008. A voxel-based lidar method for estimating crown base height for deciduous and pine trees. Remote Sensing of Environment 112, 767–781. https://doi.org/10.1016/j.rse.2007.06.011

Pretzsch, H., 1995. Zum Einfluß des Baumverteilungsmusters auf den Bestandeszuwachs.

Romeiro, J.M.N., Strîmbu, V.F., Eid, T., Kangas, A., 2025. Optimizing forest management in the face of bark beetle risk. Ecological Modelling 507, 111160. https://doi.org/10.1016/j.ecolmodel.2025.111160

Roussel, J.-R., Auty, D., De Boissieu, F., Sanchez Meador, A., Bourdon, J.-F., Gatziolis, D., 2021. Package ‘ lidR .’

Sharma, R.P., Vacek, Z., Vacek, S., Podrázský, V., Jansa, V., 2017. Modelling individual tree height to crown base of Norway spruce (Picea abies (L.) Karst.) and European beech (Fagus sylvatica L.). PLoS One 12, e0186394. https://doi.org/10.1371/journal.pone.0186394

Souden, S., Ennajeh, M., Ouledali, S., Massoudi, N., Cochard, H., Khemira, H., 2020. Water relations, photosynthesis, xylem embolism and accumulation of carbohydrates and cyclitols in two Eucalyptus species (E. camaldulensis and E. torquata) subjected to dehydration–rehydration cycle. Trees 34, 1439–1452. https://doi.org/10.1007/s00468-020-02016-4

Terryn, L., Calders, K., Åkerblom, M., Bartholomeus, H., Disney, M., Levick, S., Origo, N., Raumonen, P., Verbeeck, H., 2023. Analysing individual 3D tree structure using the R package ITSMe. Methods in Ecology and Evolution 14, 231–241. https://doi.org/10.1111/2041-210X.14026

Wollschlaeger, D., 2025. shotGroups: Analyze Shot Group Data.